processes

MDPI

*Article*

# Exact Linearization and Trajectory Tracking for a 3DOF Helicopter

**Jorge Guillermo Alonso-Alfaro [1], Salvador Antonio Rodríguez-Paredes [1,*], Jesús Martínez-Martínez [2], Bernardino Benito Salmerón-Quiroz [1] and José Manuel Gallardo-Villarreal [3]**

[1] SEPI ESIME Azcapotzalco, Instituto Politécnico Nacional, Calz. Azcapotzalco—La Villa, El Jaguey, Azcapotzalco, Ciudad de México 02519, Mexico; jorgealonsoalfaro@gmail.com (J.G.A.-A.); bsalmeron@ipn.mx (B.B.S.-Q.)
[2] Tecnológico de Estudios Superiores de Huixquilucan, Tecnológico Nacional de México, Paraje El Río s/n, Col. La Magdalena Chichiscapa, Huixquilucan 52773, Estado de México, Mexico; jesus.m.m@huixquilucan.tecnm.mx
[3] Colegio de Ciencias y Humanidades, Universidad Nacional Autónoma de México, Coyoacán, Ciudad de México 04510, Mexico; jmgv@comunidad.unam.mx
* Correspondence: sarodriguezp@ipn.mx

**Abstract**

This paper presents the design of a control strategy based on exact feedback linearization and dynamic stabilization for the mathematical model of a benchmark Quanser platform emulating the elevation, pitch, and travel motions of a three-degree-of-freedom (3-DOF) tandem helicopter. The orientation dynamics of the aerial vehicle are described by a set of highly coupled, inherently unstable nonlinear differential equations. Unlike conventional feedback linearization approaches, the core contribution of this work lies in a strategic subsystem decoupling technique combined with a symmetric input transformation and a formal proof of exact linearizability. Once the exact linear canonical representation is derived, optimal Linear Quadratic Regulator (LQR) control gains are synthesized directly within the transformed coordinates. Subsequently, a trajectory tracking scheme is developed for each degree of freedom, simulating aggressive trajectory changes that emulate obstacle-avoidance maneuvers during a mission. Numerical simulations in MATLAB/Simulink demonstrate that the proposed control scheme achieves precise tracking and rapid stabilization while strictly adhering to the physical angular bounds of the experimental platform and operational actuator constraints.

**Keywords:** nonlinear systems; 3DOF tandem helicopter; exact feedback linearization; stabilization; trajectory tracking

Check for updates

Academic Editor: Dan Zhang

Received: 11 July 2026
Revised: 5 September 2026
Accepted: 7 September 2026
Published: 15 September 2026

**Copyright:** © 2026 by the authors. Licensee MDPI, Basel, Switzerland. This article is an open access article distributed under the terms and conditions of the Creative Commons Attribution (CC BY) license.

## 1. Introduction

Unmanned Aerial Vehicles (UAVs), also known as Remotely Piloted Aircraft Systems (RPAS) [1], have become widely used in civil [2], surveillance [3], and military applications. According to ICAO standards, RPAS refer to unmanned aircraft that are piloted from a remote pilot station. These systems may include varying levels of onboard automation to assist flight and mission execution; however, control authority remains with a human operator located outside the aircraft [4].

RPAS can be classified in different ways, either by their configuration—namely fixed-wing, rotary-wing, or airships—or commonly by their weight [5,6]. For these reasons, there is a wide variety of topics in which they are studied. For example, configurations aimed

at optimizing energy resources; hybrid configurations between vehicles that normally behave as fixed-wing aircraft but, through a change in rotor configuration, can operate as rotary-wing aircraft [7]; material selection to reduce weight while preserving the desired mechanical characteristics [8]; the design of control strategies for specific missions [9]; trajectory design for electric vertical takeoff and landing (eVTOL) [10]; design of optimal deployment algorithms [11]; and the design of experimental platforms to validate some of the aforementioned approaches [12], among others.

In this article, the object of study focuses on the design of a control strategy for the Quanser 3DOF experimental platform [13], in which it is possible to represent the orientation dynamics (yaw, pitch, and roll) of a tandem helicopter. Experimental platforms play a significant role in both industrial and academic sectors, as they allow the experimental validation of various innovations related to RPAS without risking the physical integrity of people or the unmanned aerial vehicles themselves, while also enabling continuous reuse.

Several research works related to the Quanser 3DOF helicopter have been reported. In some of them, an approximate linearization of the tandem helicopter's mathematical model is first performed [13,14], followed by the design of a control strategy. Other works are based on feedback linearization techniques [15,16], as well as on the development of nonlinear control strategies [17–19].

The Quanser 3DOF helicopter platform consists of two DC motors mounted at the ends of a helicopter-shaped frame. Two propellers are attached to the motor shafts, which, together with the motors, represent the front and rear rotors of the aircraft; these actuators constitute the inputs of the plant. The helicopter frame is suspended by means of a long rod and supported by a measuring instrument that allows the pitch angle of the vehicle to be measured with respect to the instrument axis. This configuration also allows the tandem to travel freely.

The rotor axes are parallel and generate a thrust force normal to the frame. When a positive voltage is supplied to the front rotor, a positive pitch motion is generated; if a positive voltage is applied to the rear rotor, the pitch motion is in the negative direction. A positive voltage applied to both motors produces elevation of the body. At the opposite end of the long rod, there is a counterweight such that the mass of the aircraft is lower than that of the counterweight; therefore, the thrust force generated by the rotors allows the tandem to be lifted.

In this work, exact feedback linearization is proposed for the tandem helicopter with the objective of stabilizing the system and designing a trajectory-tracking control strategy for the aerial vehicle. Initially, the nonlinear three-degree-of-freedom (3DOF) dynamic model is presented, describing the vehicle's behavior in elevation, pitch, and travel motions. The model consists of a system of nonlinear differential equations and represents an unstable system. Subsequently, the parameters associated with the platform architecture are introduced.

A symmetric transformation is then employed in order to partially decouple the system dynamics, resulting in two nonlinear subsystems that are analyzed independently. For each subsystem, the conditions for exact linearization are studied through the analysis of the relative degree and the distributions generated by the associated Lie vector fields [20]. In the case of the subsystem corresponding to pitch and travel motions, it is verified that the Lie distributions satisfy the necessary involutivity conditions [20,21], thereby guaranteeing the existence of a linear transformation structured by a pure integrator chain.

Once exact linearization of the subsystems is established, a feedback control law is implemented to achieve algebraic cancellation of the nonlinearities and obtain an equivalent linear dynamic model. Based on the linearized model, control gains are designed to ensure closed-loop stabilization of the subsystems. Finally, a trajectory-tracking control strategy is

developed, based on the linearized model and applied to the nonlinear system for elevation, pitch, and travel motions.

## 2. Mathematical Modeling and Decoupling

Considering Figure 1 and denote the angles as follows: $\theta_e$ for elevation, $\theta_t$ for travel (yaw), and $\theta_p$ for the pitch of the 3DOF Tandem Helicopter [22]. From the free-body diagram shown in Figure 1, the following differential equations are obtained, which describe the dynamics of the 3DOF Helicopter:

$$J_e\ddot{\theta}_e = l_a\left(f_f + f_b\right) - l_w f_g \cos\theta_e \tag{1}$$

$$J_t\ddot{\theta}_t = -l_a k_p \sin\theta_p \tag{2}$$

$$J_p\ddot{\theta}_p = l_h\left(f_f - f_b\right) \tag{3}$$

where $J_e$, $J_t$, and $J_p$ denote the moments of inertia with respect to the elevation, travel, and pitch axes, respectively; $l_a$, $l_h$ and $l_w$ are lengths shown in Figure 1; $m_f$, $f_f$, $m_b$, $f_b$, $m_h$, $f_g$ and $m_w$ are the forces acting on the helicopter at the front, rear, and due to gravity $g$, respectively. Table 1 presents the parameter values assigned to the system, taken directly from the manufacturer's manual.

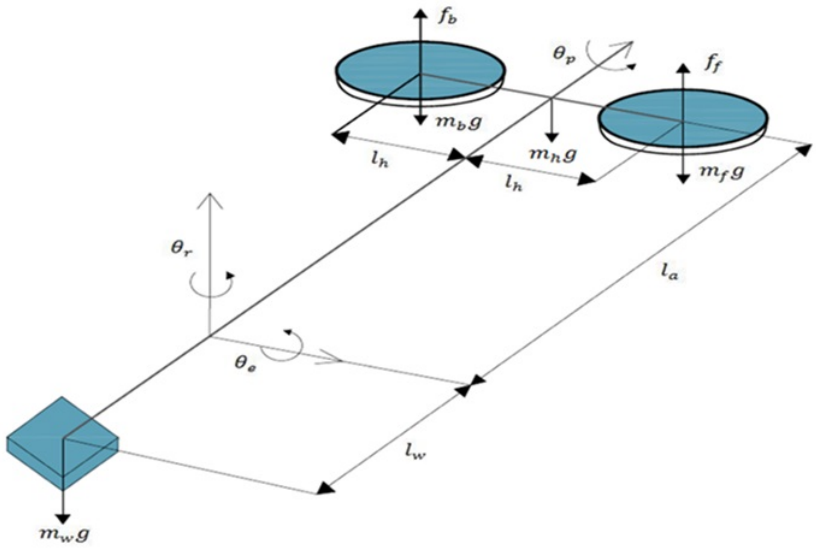



**Figure 1.** Free-body diagram of the 3-DOF helicopter.

**Table 1.** 3-DOF Tandem Helicopter Parameters [13].

| Symbol | Description | Value |
|---|---|---|
| $J_e$ | Elevation moment of inertia | 0.91 kg·m$^2$ |
| $J_t$ | Travel moment of inertia | 0.91 kg·m$^2$ |
| $J_p$ | Pitch moment of inertia | 0.034 kg·m$^2$ |
| $l_a$ | Distance from pivot to helicopter center of mass | 0.660 m |
| $l_h$ | Distance from pivot to either rotor center of mass | 0.178 m |
| $l_w$ | Distance from pitch axis to counterweight | 0.47 m |
| $k$ | Motor thrust constant | 0.5 N/V |
| $k_p$ | Force required to keep the body elevated | 0.686 N |
| $v_f$ | Maximum voltage of the front motor | 5 V |
| $v_b$ | Maximum voltage of the rear motor | 5 V |

Values obtained from the manufacturer's manual [13].

Equations (1)–(3) correspond to a system of nonlinear differential equations in which the equations are coupled both in the states and in the control inputs of the system. Therefore, an appropriate change of variables in the control inputs is proposed to decouple the system into two separate dynamics. For this purpose, the force terms are rewritten as follows: $f_f = k_f v_f$, $f_b = k_b v_b$ with $k = k_f = k_b$, and $f_g = k_p l_a / l_w$.

A symmetric transformation in terms of $u_f$ and $u_b$ is then employed [23], introducing two new control variables with the following structure:

$$\begin{bmatrix} v_f \\ v_b \end{bmatrix} = \begin{bmatrix} -\frac{1}{2} & \frac{1}{2} \\ \frac{1}{2} & \frac{1}{2} \end{bmatrix} \begin{bmatrix} u_f \\ u_b \end{bmatrix} \tag{4}$$

Substituting Equation (4) into the system of Equations (1) and (3) allows rewrite (1)–(3) as follows:

$$J_e \ddot{\theta}_e = l_a k u_b - l_w f_g \cos\theta_e \tag{5}$$

$$J_t \ddot{\theta}_t = -l_a k_p \sin\theta_p \tag{6}$$

$$J_p \ddot{\theta}_p = -l_h k u_f \tag{7}$$

The system (5)–(7) is no longer coupled through the control inputs and can therefore be divided into two subsystems as follows: Equation (5) depends only on $\theta_e$ and the auxiliary control signal $u_b$; on the other hand, Equations (6) and (7) are coupled through $\theta_p$ and depend only on the new auxiliary control signal $u_f$. The problem is thus simplified for the study of structural properties and the design of control strategies to manipulate the dynamics of the 3DOF Tandem Helicopter.

## 3. Exact Linearization

In this section, the exact linearization of the decoupled nonlinear model of the three-degree-of-freedom (3DOF) helicopter is shown, as described by Equations (4)–(6) through a set of nonlinear differential equations. The linearization process is carried out independently for each subsystem, taking advantage of the decoupled structure of the model. First, the elevation subsystem is addressed. Subsequently, the linearization of the subsystem associated with the pitch and travel dynamics is performed, considering their possible interactions.

### *3.1. Exact Linearization (Elevation)*

Equation (5) describes the behavior of the tandem helicopter with respect to the elevation angle $\theta_e$. To achieve exact feedback linearization, we define an auxiliary virtual control input $v_b$ such that $\ddot{\theta}_e = v_b$. By substituting this condition into Equation (5) and solving algebraically for $u_b$, we obtain

$$J_e v_b = l_a k u_b - l_w f_g \cos\theta_e \tag{8}$$

Consequently, the linearizing control law that cancels the system nonlinearities is derived as follows:

$$u_b = \frac{J_e}{l_a k}\left(\frac{l_w f_g}{J_e}\cos\theta_e + v_b\right) \tag{9}$$

To incorporate an integral action into the state-space representation, a dynamic extension of the elevation subsystem is performed. Specifically, an auxiliary state variable $\zeta$ is defined as the integral of the elevation angle $\theta_e$:

$$\dot{\zeta} := \theta_e \implies \zeta(t) = \int_0^t \theta_e(\tau)\, d\tau \tag{10}$$

By incorporating $\zeta$ alongside the physical states $\theta_e$ and $\dot{\theta}_e$, the system is dynamically extended into a third-order state-space model. This dynamic extension introduces a PID structure directly into the state-space formulation, ensuring zero steady-state tracking error.

Consequently, the augmented linear state-space model is formulated as expressed in Equation (11):

$$\begin{bmatrix} \dot{\zeta} \\ \dot{\theta}_e \\ \ddot{\theta}_e \end{bmatrix} = \begin{bmatrix} 0 & 1 & 0 \\ 0 & 0 & 1 \\ 0 & 0 & 0 \end{bmatrix} \begin{bmatrix} \zeta \\ \theta_e \\ \dot{\theta}_e \end{bmatrix} + \begin{bmatrix} 0 \\ 0 \\ 1 \end{bmatrix} v_b \tag{11}$$

### *3.2. Exact Linearization (Pitch and Travel)*

For the subsystem described by Equations (6) and (7), corresponding to the travel and pitch dynamics of the helicopter, it is not possible to obtain a linearizing control law by simple inspection. Therefore, it is necessary to determine a function $h(x)$ such that it generate a transformed system in such a way that an exact linearizing control law can be designed.

To this end, the existence of the function $h(x)$ must be verified.

Let $h(x)$ be a transformation function defined locally around a point $x$ in the state space, capable of reducing the system to controllable canonical form. The function $h(x)$ exists if and only if the following conditions are satisfied [21]:

1. The set of vectors
$$\left\{ g,\ ad_f g,\ ad_f^2 g,\ \ldots,\ ad_f^{n-1} g \right\}$$
is locally linearly independent around $x$.
2. The subset of vector fields
$$\left\{ g,\ ad_f g,\ ad_f^2 g,\ \ldots,\ ad_f^{n-2} g \right\}$$
is locally involutive. Let
$$g^T = \begin{bmatrix} 0 & 0 & 0 & -\frac{l_h k}{J_p} \end{bmatrix} \tag{12}$$
$$f = \begin{bmatrix} \omega_t \\ -\frac{l_a k_p}{J_t} \sin\theta_p \\ \omega_p \\ 0 \end{bmatrix} \tag{13}$$
were $\omega_t = \dot{\theta}_t$ and $\omega_p = \dot{\theta}_p$.

To verify Condition 1, the Lie brackets of $f$ and $g$ must be computed as follows:

$$ad_f g = [f, g] = \frac{\partial g}{\partial x} f - \frac{\partial f}{\partial x} g \tag{14}$$
$$ad_f^n g = \left[ f, ad_f^{n-1} g \right], \quad n \geqslant 1 \tag{15}$$
$$ad_f g = \begin{bmatrix} 0 \\ 0 \\ \frac{l_h k}{J_p} \\ 0 \end{bmatrix} \tag{16}$$
$$ad_f^2 g = \left[ f, ad_f g \right] = \begin{bmatrix} 0 \\ -\frac{l_h k}{J_p} \frac{l_a k_p}{J_t} \cos\theta_p \\ 0 \\ 0 \end{bmatrix} \tag{17}$$

$$ad_f^3 g = \left[f, ad_f^2 g\right] = \begin{bmatrix} \frac{l_h k}{J_p}\frac{l_a k_p}{J_t}\cos\theta_p \\ \frac{l_h k}{J_p}\frac{l_a k_p}{J_t}\omega_p \sin\theta_p \\ 0 \\ 0 \end{bmatrix} \tag{18}$$

Concatenating the vectors from Equations (12), (16)–(18) yields the following matrix arrangement:

$$\longleftrightarrow \left\{ \begin{bmatrix} 0 \\ 0 \\ 0 \\ -\frac{l_h k}{J_p} \end{bmatrix}, \begin{bmatrix} 0 \\ 0 \\ \frac{l_h k}{J_p} \\ 0 \end{bmatrix}, \begin{bmatrix} 0 \\ -\frac{l_h k}{J_p}\frac{l_a k_p}{J_t}\cos\theta_p \\ 0 \\ 0 \end{bmatrix}, \begin{bmatrix} \frac{l_h k}{J_p}\frac{l_a k_p}{J_t}\cos\theta_p \\ \frac{l_h k}{J_p}\frac{l_a k_p}{J_t}\omega_p \sin\theta_p \\ 0 \\ 0 \end{bmatrix} \right\} \tag{19}$$

where $\theta_p \neq \frac{\pi}{2} + \kappa\pi, \kappa = \pm 0, \pm 1, \pm 2, \ldots$

$$rank\left\{ g(x_0), ad_f g(x_0), ad_f^2 g(x_0), ad_f^3 g(x_0) \right\} = 4 \tag{20}$$

The vectors in Equation (19) are linearly independent. Therefore, the rank of the matrix in Equation (20) is full, which verifies that Condition 1 is satisfied.

Next, Condition 2 is analyzed in order to determine whether there exists a transformation that exactly linearizes the system defined by Equations (6) and (7).

Consider

$$g \times ad_f g = 0 \tag{21}$$

$$g \times ad_f^2 g = \left[\frac{\partial}{\partial x} ad_f^2 g\right] g - \frac{\partial g}{\partial x} ad_f^2 g = 0 \tag{22}$$

$$ad_f g \times ad_f^2 g = \begin{bmatrix} 0 \\ -\frac{l_h k}{J_p}\frac{l_a k_p}{J_t}\sin\theta_p \\ 0 \\ 0 \end{bmatrix} \tag{23}$$

Thus, $\delta = \left\{ g, ad_f g, ad_f^2 g \right\}$ is involutive.

$$\longleftrightarrow \left\{ \begin{bmatrix} 0 \\ 0 \\ 0 \\ -\frac{l_h k}{J_p} \end{bmatrix}, \begin{bmatrix} 0 \\ 0 \\ \frac{l_h k}{J_p} \\ 0 \end{bmatrix}, \begin{bmatrix} 0 \\ -\frac{l_h k}{J_p}\frac{l_a k_p}{J_t}\cos\theta_p \\ 0 \\ 0 \end{bmatrix}, \begin{bmatrix} 0 \\ -\frac{l_h k}{J_p}\frac{l_a k_p}{J_t}\sin\theta_p \\ 0 \\ 0 \end{bmatrix} \right\} \langle \forall \theta_p \rangle \tag{24}$$

$$rank\left\{ \begin{bmatrix} 0 \\ 0 \\ 0 \\ -\frac{l_h k}{J_p} \end{bmatrix}, \begin{bmatrix} 0 \\ 0 \\ \frac{l_h k}{J_p} \\ 0 \end{bmatrix}, \begin{bmatrix} 0 \\ -\frac{l_h k}{J_p}\frac{l_a k_p}{J_t}\cos\theta_p \\ 0 \\ 0 \end{bmatrix}, \begin{bmatrix} 0 \\ -\frac{l_h k}{J_p}\frac{l_a k_p}{J_t}\sin\theta_p \\ 0 \\ 0 \end{bmatrix} \right\} = 3 \tag{25}$$

According to the Frobenius theorem [21], Equation (25) corresponds to an involutive system. Therefore, Conditions 1 and 2 of the Lemma in [21] are satisfied, which implies that the system can be exactly linearized.

To determine a scalar vector field $h(x)$ that generates the state transformation, the following system of partial differential equations must be satisfied:

$$\frac{\partial h}{\partial x}\left(g, ad_f g, ad_f^2 g\right) = 0 \tag{26}$$

$$\begin{bmatrix} \frac{\partial h}{\partial x_1} \\ \frac{\partial h}{\partial x_2} \\ \frac{\partial h}{\partial x_3} \\ \frac{\partial h}{\partial x_4} \end{bmatrix}^T \begin{bmatrix} 0 & 0 & 0 \\ 0 & 0 & -\frac{l_h k}{J_p}\frac{l_a k_p}{J_t}\cos\theta_p \\ 0 & -\frac{l_h k}{J_p} & 0 \\ -\frac{l_h k}{J_p} & 0 & 0 \end{bmatrix} = \begin{bmatrix} 0 \\ 0 \\ 0 \end{bmatrix}^T \tag{27}$$

Based on Equations (26) and (27), selecting the function $h(x) = x_1$ satisfies the system conditions, allowing the following linearizing transformation to be established:

$$z := \vartheta(x) = \begin{bmatrix} h(x) \\ L_f h(x) \\ L_f^2 h(x) \\ L_f^3 h(x) \end{bmatrix} \tag{28}$$

A particular solution that satisfies the previous conditions yields the explicit transformation

$$z = \begin{bmatrix} z_1 \\ z_2 \\ z_3 \\ z_4 \end{bmatrix} := \begin{bmatrix} x_1 \\ x_2 \\ -\frac{l_a k_p}{J_t}\sin x_3 \\ -\frac{l_a k_p}{J_t} x_4 \cos x_3 \end{bmatrix} \tag{29}$$

From (29), the inverse transformation that maps the state variables from $z$ to $x$ can be determined as follows:

$$z_1 = x_1 \Rightarrow x_1 = z_1 \tag{30}$$

$$z_2 = x_2 \Rightarrow x_2 = z_2 \tag{31}$$

$$z_3 = -\frac{l_a k_p}{J_t}\sin x_3 \Rightarrow x_3 = \arcsin\left(-\frac{z_3}{\frac{l_a k_p}{J_t}}\right) \tag{32}$$

$$z_4 = -\frac{l_a k_p}{J_t} x_4 \cos x_3 \Rightarrow x_4 = -\frac{z_4}{\frac{l_a k_p}{J_t}\cos x_3};\ \text{where}\ \cos x_3 \neq 0;\ -\frac{\pi}{2} < x_3 < \frac{\pi}{2}. \tag{33}$$

The transformed model can now be written in controllable canonical form as

$$\begin{bmatrix} \dot{z}_1 \\ \dot{z}_2 \\ \dot{z}_3 \\ \dot{z}_4 \end{bmatrix} = \begin{bmatrix} z_2 \\ z_3 \\ z_4 \\ \frac{l_a k_p}{J_t} x_4^2 \sin x_3 + u_f \frac{l_a k_p}{J_t}\frac{l_h k}{J_p}\cos x_3 \end{bmatrix} \tag{34}$$

It can be readily observed that system (34) can be immediately linearized. To this end, an auxiliary external control variable $v$ is introduced. In order to obtain a linear model, the control input $u$ is defined as

$$u_f = \frac{v - \frac{l_a k_p}{J_t} x_4^2 \sin x_3}{\frac{l_a k_p}{J_t}\frac{l_h k}{J_p}\cos x_3} \tag{35}$$

It can be observed that the control law presented in Equation (35) exhibits a singularity in the denominator associated with the term $\cos x_3$. Therefore, this control law is valid only when $\cos x_3 \neq 0$, a condition that holds for $-\frac{\pi}{2} < x_3 < \frac{\pi}{2}$.

From a physical standpoint, when the pitch angle reaches $\pi/2$ (90 [deg]), the rotor thrust vector completely loses its vertical alignment, failing to generate the necessary lift force. Consequently, the helicopter loses its ability to sustain elevation, rendering the

system strictly non-operational. However, due to the physical mechanical constraints of the experimental platform which restrict the pitch angle to a range of $\pm 32$ [deg] the proposed controller operates safely and effectively well within this functional regime.

Substituting (35) into (34) results in the linear system

$$\begin{bmatrix} \dot{z}_1 \\ \dot{z}_2 \\ \dot{z}_3 \\ \dot{z}_4 \end{bmatrix} = \begin{bmatrix} z_2 \\ z_3 \\ z_4 \\ v \end{bmatrix} \tag{36}$$

The resulting model exhibits a pure chain-of-integrators structure, which greatly facilitates controller design using linear control techniques.

## 4. Stabilization

### *4.1. Elevation*

The poles of the linear system shown in Equation (11) are located at the origin; therefore, the system is unstable. In order to stabilize it, a state-feedback control law is proposed, where the input $v_b$ is defined as

$$v_b = -k_e x_e = -k_{e0}\zeta - k_{e1}\theta_e - k_{e2}\dot{\theta}_e \tag{37}$$

where $x_e = [\zeta \quad \theta_e \quad \dot{\theta}_e]^T$ is the state vector of the linear system (11) corresponding to the elevation dynamics, and $k_e = [k_{e0} \quad k_{e1} \quad k_{e2}]$ is the gain vector that stabilizes the system.

To select the gains that stabilize the subsystem, the MATLAB LQR (version R2020a) command is employed. The following weighting matrix $Q$ and scalar value $R$, obtained from the manufacturer's manual [13], are proposed:

$$Q = \begin{bmatrix} 100 & 0 & 0 \\ 0 & 0 & 0 \\ 0 & 0 & 10 \end{bmatrix} \tag{38}$$

and

$$R = 0.05 \tag{39}$$

The resulting gain vector is

$$k_e = \begin{bmatrix} 44.7214 & 38.5889 & 16.6487 \end{bmatrix} \tag{40}$$

The following figures present the numerical simulation results obtained in the MATLAB/Simulink (version R2020a) environment using the Runge–Kutta integration method to validate the computed control gains for the tandem helicopter. These simulations are based on the dynamic model of the benchmark Quanser 3-DOF Helicopter platform, considering two distinct operational scenarios with different subsystem initial conditions. To preserve physical feasibility and avoid unrealistic behaviors, the Quanser platform is strictly constrained within the actual physical angular bounds of the platform across its three degrees of freedom [13]. Specifically, the pitch axis is restricted to $\theta_p \in [-32.0$ [deg], $+32.0$ [deg]], a total stroke of 64 [deg], while the elevation motion operates within a physical stroke of 63.5 [deg] ranging from $-27.5$ [deg] to $+36.0$ [deg]. In contrast, the travel axis features an unconstrained continuous 360 [deg] rotational capability. Furthermore, for all simulations, the initial conditions were proposed to lie strictly within these ranges, and all simulations conducted throughout this work adhere to these physical limits, using the system parameters listed in Table 1.

First, it is assumed that the vehicle is initially at rest with the motors turned off and positioned horizontally, that is, with $\theta_e(0) = 0$ [deg], $\theta_p(0) = 0$ [deg], $\theta_t(0) = 0$ [deg], $\dot{\theta}_e(0) = 0$ [deg/s], $\dot{\theta}_p(0) = 0$ [deg/s] and $\dot{\theta}_t(0) = 0$ [deg/s]. Additionally, it is assumed that no external disturbances are present. In Figure 2, it can be observed that due to the weight of the aerial vehicle body, $\theta_e(t)$ takes negative values in the elevation angular position for $0[s] < t < 2.5[s]$ approximately, indicating that the vehicle tends to descend due to gravitational force. Subsequently $\theta_e(t)$ increase once the motors are activated, the control law acts to stabilize the subsystem at the equilibrium point, i.e., $\theta_e = 0$ [deg], maintaining the vehicle in a horizontal position and ensuring that the lift force balances the weight of the tandem helicopter.

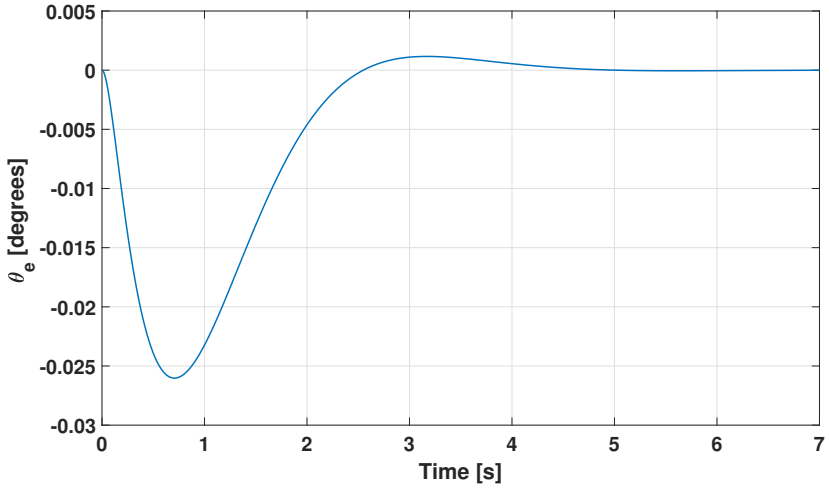
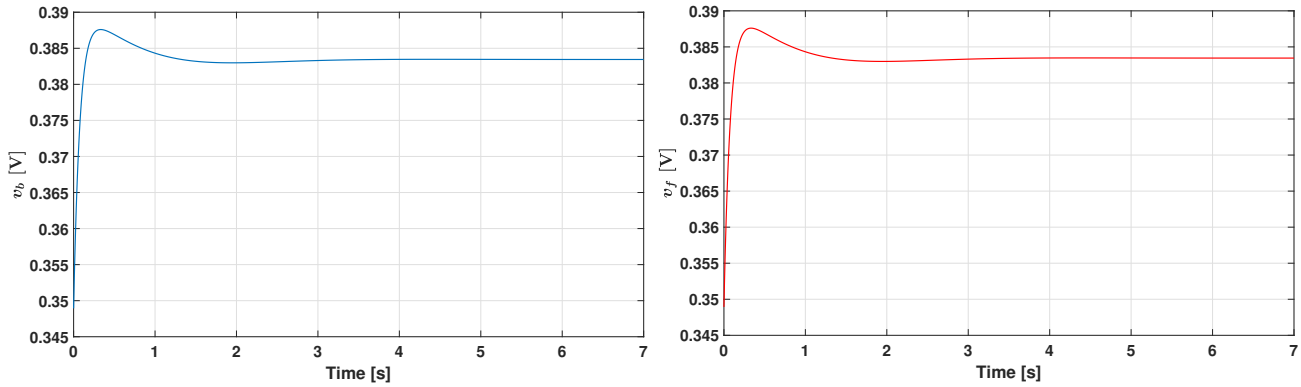



**Figure 2.** Elevation response with $\theta_e(0) = 0$ [deg], $\theta_p(0) = 0$ [deg], $\theta_t(0) = 0$ [deg], $\dot{\theta}_e(0) = 0$ [deg/s], $\dot{\theta}_p(0) = 0$ [deg/s] and $\dot{\theta}_t(0) = 0$ [deg/s], assuming constant system parameters.

In Figure 3, the voltages corresponding to the front and rear motors of the aerial vehicle are shown. Both actuators exhibit a transient response at the beginning, characterized by a small overshoot. Subsequently, both signals converge toward a value of +0.3835 V, indicating that the control action required to maintain the equilibrium condition stabilizes. Furthermore, the motor voltages remain within the maximum operating limits throughout the process.




(**a**) (**b**)

**Figure 3.** Motor voltage response during the approach of the 3-DOF tandem helicopter to its equilibrium condition with $\theta_e(0) = 0$ [deg], $\theta_p(0) = 0$ [deg], $\theta_t(0) = 0$ [deg], $\dot{\theta}_e(0) = 0$ [deg/s], $\dot{\theta}_p(0) = 0$ [deg/s] and $\dot{\theta}_t(0) = 0$ [deg/s], assuming constant system parameters: (**a**) Rear motor voltage. (**b**) Front motor voltage.

Subsequently, a nonzero initial condition is considered only for the elevation; that is, the helicopter is initially elevated with an angle $\theta_e(0) = 3$ [deg], while $\theta_p(0) = 0$ [deg], $\theta_t(0) = 0$ [deg], $\dot{\theta}_e(0) = 0$ [deg/s], $\dot{\theta}_p(0) = 0$ [deg/s] and $\dot{\theta}_t(0) = 0$ [deg/s]. Additionally, it is assumed that no external disturbances are present. In Figure 4, it can be observed that the control law acts on the system and drives the helicopter toward the equilibrium point corresponding to $\theta_e = 0$ [deg], maintaining it stable at this position.

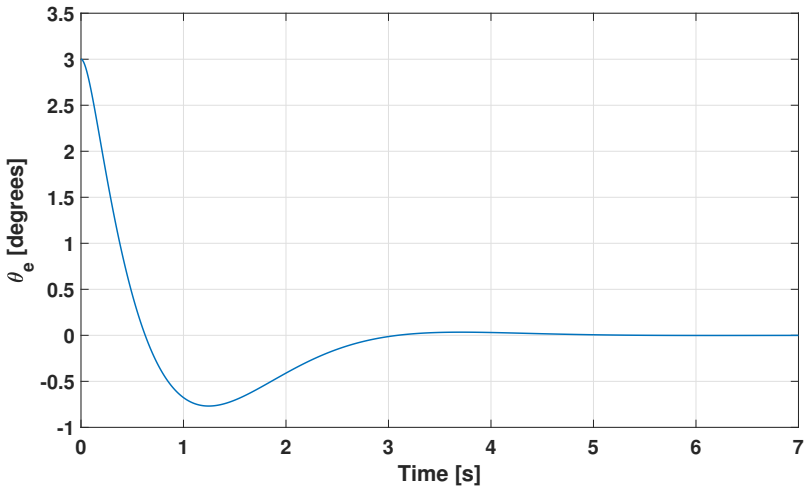
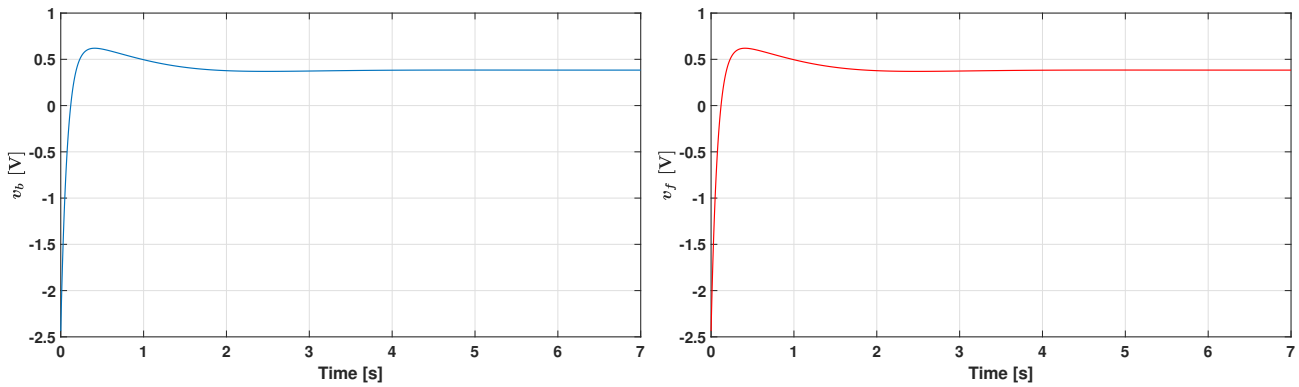



**Figure 4.** Elevation response with $\theta_e(0) = 3$ [deg], $\theta_p(0) = 0$ [deg], $\theta_t(0) = 0$ [deg], $\dot{\theta}_e(0) = 0$ [deg/s], $\dot{\theta}_p(0) = 0$ [deg/s] and $\dot{\theta}_t(0) = 0$ [deg/s], assuming constant system parameters.

Figure 5 shows the dynamic response of the control signals $v_b$ and $v_f$ over a 7 s time interval. Both variables exhibit a symmetric and smooth response to maintain the vehicle at the equilibrium point, demonstrating a coordinated control performance between the actuators. At the beginning of the simulation ($t = 0$ s), an initial transient peak of $-2.5$ V occurs, attributed to rapid compensation for the initial position error. Subsequently, the signals respond with a moderate overshoot of $+0.62$ V around $t = 0.35$ s, followed by progressive damping that stabilizes the system after 3 s at a steady-state value of $+0.3835$ V. The absence of high-frequency oscillations or prolonged saturation evidences suitable controller performance, keeping the effort within appropriate operational limits for the motors.




(**a**) (**b**)

**Figure 5.** Motor voltage response during the approach of the 3-DOF tandem helicopter to its equilibrium condition with $\theta_e(0) = 3$ [deg], $\theta_p(0) = 0$ [deg], $\theta_t(0) = 0$ [deg], $\dot{\theta}_e(0) = 0$ [deg/s], $\dot{\theta}_p(0) = 0$ [deg/s] and $\dot{\theta}_t(0) = 0$ [deg/s], assuming constant system parameters: (**a**) Rear motor voltage. (**b**) Front motor voltage.

*4.2. Pitch and Travel*

By selecting $v$ as in Equation (37), corresponding to linear state feedback, asymptotic regulation of the subsystem is guaranteed.

$$v = -k_t z = -k_{t0} z_1 - k_{t1} z_2 - k_{t2} z_3 - k_{t3} z_4 \tag{41}$$

where $z$ is the state vector of the transformed linear system (36) associated with the pitch and travel dynamics, and $k_t = [k_{t0} \;\; k_{t1} \;\; k_{t2} \;\; k_{t3}]$ is the gain vector that stabilizes the system.

To obtain the gains that stabilize the pitch and travel subsystem, the MATLAB LQR command is again employed. The following weighting matrix $Q$ and scalar value $R$, obtained from the manufacturer's manual [13], are proposed:

$$Q = \begin{bmatrix} 10 & 0 & 0 & 0 \\ 0 & 2 & 0 & 0 \\ 0 & 0 & 1 & 0 \\ 0 & 0 & 0 & 0 \end{bmatrix} \tag{42}$$

and

$$R = 0.05 \tag{43}$$

The resulting gain vector is

$$k_t = \begin{bmatrix} 14.1421 & 21.6658 & 15.1818 & 5.5103 \end{bmatrix} \tag{44}$$

Finally, substituting $v$ from Equation (41) into Equation (35) yields

$$u_f = \frac{(-k_{t0} z_1 - k_{t1} z_2 - k_{t2} z_3 - k_{t3} z_4) - \frac{l_a k_p}{J_t} x_4^2 \sin x_3}{\frac{l_a k_p}{J_t} \frac{l_h k}{J_p} \cos x_3} \tag{45}$$

To validate the LQR gains obtained for the pitch and travel control law, non-zero initial conditions are established for the pitch state, with $\theta_e(0) = 0$ [deg], $\theta_p(0) = 30$ [deg], $\theta_t(0) = 0$ [deg], $\dot{\theta}_e(0) = 0$ [deg/s], $\dot{\theta}_p(0) = 0$ [deg/s], and $\dot{\theta}_t(0) = 0$ [deg/s]. In Figures 6 and 7, it can be observed that, under the action of the control law described in Equation (45), the subsystem converges to the equilibrium points $\theta_p = 0$ [deg] and $\theta_t = 0$ [deg], remaining stable once equilibrium is reached.

Figure 8 shows the dynamic response of the control voltages $v_b(t)$ and $v_f(t)$ applied to the 3 DOF tandem helicopter over a 7 s period. Unlike the symmetrical response obtained in the elevation simulation, the initial signals reflect the asymmetry required by the control action to compensate for the system's initial conditions in pitch, while $v_b$ starts from a positive value of $+2$ V, $v_f$ begins at a negative level of $-1.35$ V. Following the initial compensation phase, both signals exhibit damped behavior, reaching transient peaks of $+0.48$ V at $t = 2.2$ s for $v_b$, and $+0.78$ V at $t = 0.8$ s for $v_f$. Finally, the coordinated action of the actuators enables the system to converge smoothly to a steady-state value of $+0.3835$ V after 4 s, ensuring stability around the equilibrium point without high-frequency oscillations or saturation.

To quantitatively evaluate the stabilization performance of the proposed controller, the root-mean-square error (RMSE), maximum absolute error, settling time, and steady-state error were calculated directly from the simulation data. The stabilization error was

defined with respect to the desired equilibrium condition. The RMSE was calculated over the complete simulation interval according to

$$\text{RMSE} = \sqrt{\frac{1}{N}\sum_{k=1}^{N} e^2(k)}, \tag{46}$$

where $e(k)$ denotes the stabilization error and $N$ is the total number of simulation samples. The maximum absolute error corresponds to the largest magnitude of the stabilization error during the transient response. The settling time was determined as the time required for the response to converge to and remain around the desired equilibrium, while the steady-state error was evaluated from the final portion of the simulation. The resulting quantitative stabilization metrics are summarized in Table 2.

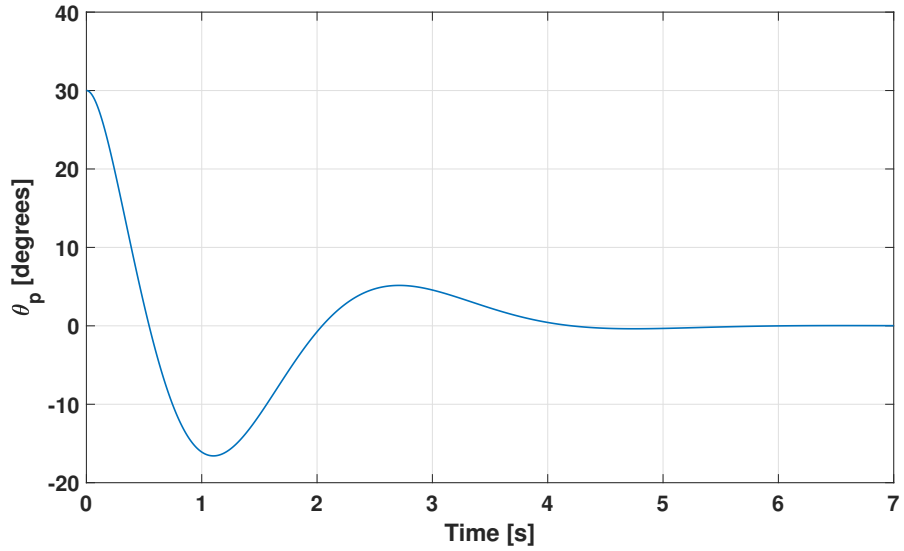



**Figure 6.** Pitch response of the 3-DOF helicopter: with $\theta_e(0) = 0$ [deg], $\theta_p(0) = 30$ [deg], $\theta_t(0) = 0$ [deg], $\dot{\theta}_e(0) = 0$ [deg/s], $\dot{\theta}_p(0) = 0$ [deg/s] and $\dot{\theta}_t(0) = 0$ [deg/s], assuming constant system parameters.

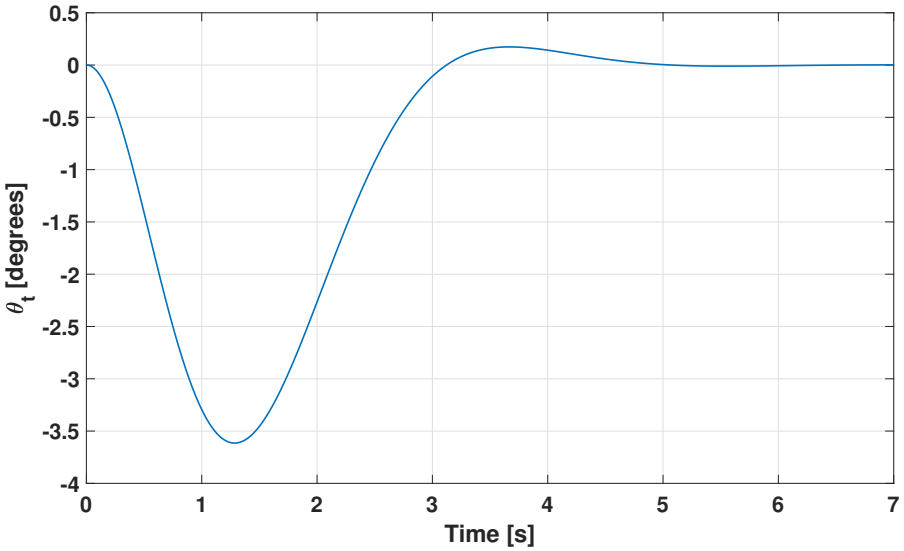
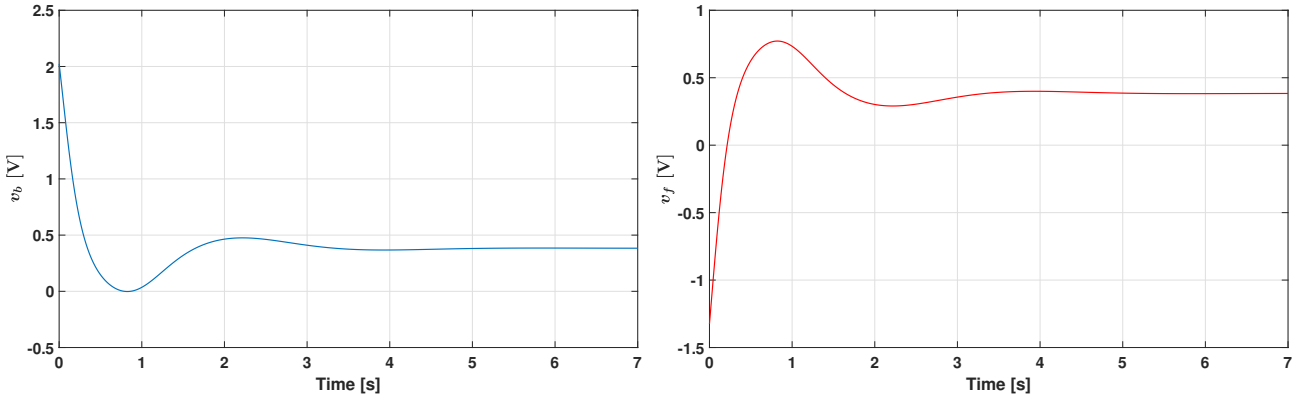



**Figure 7.** Travel response of the 3-DOF helicopter: with $\theta_e(0) = 0$ [deg], $\theta_p(0) = 30$ [deg], $\theta_t(0) = 0$ [deg], $\dot{\theta}_e(0) = 0$ [deg/s], $\dot{\theta}_p(0) = 0$ [deg/s] and $\dot{\theta}_t(0) = 0$ [deg/s], assuming constant system parameters.




(**a**) (**b**)

**Figure 8.** Motor voltage response during the approach of the 3-DOF tandem helicopter to its equilibrium condition with $\theta_e(0) = 0$ [deg], $\theta_p(0) = 30$ [deg], $\theta_t(0) = 0$ [deg], $\dot{\theta}_e(0) = 0$ [deg/s], $\dot{\theta}_p(0) = 0$ [deg/s] and $\dot{\theta}_t(0) = 0$ [deg/s], assuming constant system parameters: (**a**) Rear motor voltage. (**b**) Front motor voltage.

**Table 2.** Quantitative stabilization performance of the 3-DOF tandem helicopter.

| Figure | Variable | RMSE | Maximum Error | Settling Time | Steady-State Error |
|---|---|---|---|---|---|
| Figure 2 | Elevation (deg) | 0.009600 | 0.026026 | 3.509000 | −0.000018 |
| Figure 4 | Elevation (deg) | 0.590001 | 3.000007 | 6.7760 | −0.001142 |
| Figure 6 | Pitch (deg) | 1.483609 | 3.614941 | 7.0000 | 0.000167 |
| Figure 7 | Travel (deg) | 7.799265 | 30.000013 | 7.0000 | 0.028871 |

The reported metrics were calculated directly from the simulation data corresponding to each stabilization response.

The results in Table 2 show that the proposed controller achieves accurate stabilization of the helicopter states. In particular, the steady-state errors remain close to zero for the elevation, pitch, and travel responses, indicating that the controller effectively eliminates the residual error after the transient response. The RMSE and maximum absolute error values quantify the transient deviation from the desired equilibrium, while the settling-time results provide a direct measure of the convergence rate.

## 5. Trajectory Tracking

### *5.1. Stability Analysis via Lyapunov Theory*

**Theorem 1** (Lyapunov's Direct Method [24]). *Consider an autonomous non-linear system* $\dot{\mathbf{e}} = f(\mathbf{e})$, *where* $f : D \to \mathbb{R}^n$ *is continuously differentiable on an open domain* $D \subset \mathbb{R}^n$ *containing the origin* $\mathbf{e} = \mathbf{0}$. *Let* $V : D \to \mathbb{R}$ *be a continuously differentiable function such that:*

*(i)* $V(\mathbf{0}) = 0$,
*(ii)* $V(\mathbf{e}) > 0, \quad \forall \mathbf{e} \in D \setminus \{\mathbf{0}\}$,
*(iii)* $\dot{V}(\mathbf{e}) < 0, \quad \forall \mathbf{e} \in D \setminus \{\mathbf{0}\}$.

*Then, the equilibrium point* $\mathbf{e} = \mathbf{0}$ *is asymptotically stable. Furthermore, if* $D = \mathbb{R}^n$ *and* $V(\mathbf{e})$ *is radially unbounded (i.e.,* $V(\mathbf{e}) \to \infty$ *as* $\|\mathbf{e}\| \to \infty$*), then the equilibrium point is globally asymptotically stable.*

Let the tracking errors be defined as

$$e_1 = \zeta_d - \zeta, \quad e_2 = \theta_{ed} - \theta_e, \quad e_3 = \dot{\theta}_{ed} - \dot{\theta}_e, \tag{47}$$

$$e_4 = z_{1d} - z_1, \quad e_5 = z_{2d} - z_2, \quad e_6 = z_{3d} - z_3, \quad e_7 = z_{4d} - z_4. \tag{48}$$

Thus, the error vector is given by

$$\mathbf{e} = \begin{bmatrix} e_1 & e_2 & e_3 & e_4 & e_5 & e_6 & e_7 \end{bmatrix}^T. \tag{49}$$

After applying exact feedback linearization, the tracking error dynamics can be expressed as

$$\dot{\mathbf{e}} = A\mathbf{e} + B\mathbf{w}, \tag{50}$$

where

$$A = \begin{bmatrix} 0 & 1 & 0 & 0 & 0 & 0 & 0 \\ 0 & 0 & 1 & 0 & 0 & 0 & 0 \\ 0 & 0 & 0 & 0 & 0 & 0 & 0 \\ 0 & 0 & 0 & 0 & 1 & 0 & 0 \\ 0 & 0 & 0 & 0 & 0 & 1 & 0 \\ 0 & 0 & 0 & 0 & 0 & 0 & 1 \\ 0 & 0 & 0 & 0 & 0 & 0 & 0 \end{bmatrix}, \quad B = \begin{bmatrix} 0 & 0 \\ 0 & 0 \\ 1 & 0 \\ 0 & 0 \\ 0 & 0 \\ 0 & 0 \\ 0 & 1 \end{bmatrix}, \quad \mathbf{w} = \begin{bmatrix} v_e \\ v_p \end{bmatrix}. \tag{51}$$

The system can be decomposed into two decoupled subsystems:

$$\mathbf{e}_e = \begin{bmatrix} e_1 \\ e_2 \\ e_3 \end{bmatrix}, \quad \mathbf{e}_p = \begin{bmatrix} e_4 \\ e_5 \\ e_6 \\ e_7 \end{bmatrix}. \tag{52}$$

The control inputs are defined as

$$v_e = -k_e \mathbf{e}_e, \quad v_p = -k_t \mathbf{e}_p, \tag{53}$$

where

$$k_e = \begin{bmatrix} 44.7214 & 38.5889 & 16.6487 \end{bmatrix}, \tag{54}$$

$$k_t = \begin{bmatrix} 14.1421 & 21.6658 & 15.1818 & 5.5103 \end{bmatrix}. \tag{55}$$

Substituting the control law $\mathbf{w} = -K\mathbf{e}$ yields the closed-loop error dynamics

$$\dot{\mathbf{e}} = (A - BK)\mathbf{e}, \tag{56}$$

where the block-diagonal gain matrix $K \in \mathbb{R}^{2\times 7}$ is given by

$$K = \begin{bmatrix} k_e & \mathbf{0}_{1\times 4} \\ \mathbf{0}_{1\times 3} & k_t \end{bmatrix}. \tag{57}$$

Due to the decoupled structural property, the closed-loop system can be rewritten as

$$\dot{\mathbf{e}}_e = A_e \mathbf{e}_e, \quad \dot{\mathbf{e}}_p = A_p \mathbf{e}_p, \tag{58}$$

where

$$A_e = \begin{bmatrix} 0 & 1 & 0 \\ 0 & 0 & 1 \\ -44.7214 & -38.5889 & -16.6487 \end{bmatrix}, \tag{59}$$

$$A_p = \begin{bmatrix} 0 & 1 & 0 & 0 \\ 0 & 0 & 1 & 0 \\ 0 & 0 & 0 & 1 \\ -14.1421 & -21.6658 & -15.1818 & -5.5103 \end{bmatrix}. \tag{60}$$

The characteristic polynomial of $A_e$ is

$$s^3 + 16.6487s^2 + 38.5889s + 44.7214 = 0, \tag{61}$$

with eigenvalues

$$\lambda(A_e) = \{-14.14395,\ -1.25237 \pm j1.26231\}. \tag{62}$$

For $A_p$, the characteristic polynomial is

$$s^4 + 5.5103s^3 + 15.1818s^2 + 21.6658s + 14.1421 = 0, \tag{63}$$

with eigenvalues

$$\lambda(A_p) = \{-1.22323 \pm j1.77171,\ -1.53192 \pm j0.83917\}. \tag{64}$$

Since all eigenvalues have strictly negative real parts, both $A_e$ and $A_p$ are Hurwitz matrices.

By choosing symmetric positive-definite matrices $Q_e = I_3$ and $Q_p = I_4$, the algebraic Lyapunov equations

$$A_e^T P_e + P_e A_e = -I_3, \tag{65}$$

$$A_p^T P_p + P_p A_p = -I_4 \tag{66}$$

yield unique positive-definite solutions:

$$P_e = \begin{bmatrix} 2.95910 & 1.68105 & 0.01118 \\ 1.68105 & 2.21973 & 0.05652 \\ 0.01118 & 0.05652 & 0.03343 \end{bmatrix}, \tag{67}$$

$$P_p = \begin{bmatrix} 4.69251 & 5.51544 & 2.38158 & 0.03536 \\ 5.51544 & 9.46096 & 4.84470 & 0.27765 \\ 2.38158 & 4.84470 & 4.00977 & 0.35205 \\ 0.03536 & 0.27765 & 0.35205 & 0.15463 \end{bmatrix}. \tag{68}$$

Consider the positive-definite quadratic Lyapunov candidate function:

$$V(\mathbf{e}) = \mathbf{e}_e^T P_e \mathbf{e}_e + \mathbf{e}_p^T P_p \mathbf{e}_p. \tag{69}$$

Since $P_e > 0$ and $P_p > 0$, it guarantees that

$$V(\mathbf{e}) > 0, \quad \forall \mathbf{e} \neq \mathbf{0}. \tag{70}$$

The time derivative of $V(\mathbf{e})$ along the closed-loop error trajectories is computed as

$$\dot{V}(\mathbf{e}) = \mathbf{e}_e^T (A_e^T P_e + P_e A_e)\mathbf{e}_e + \mathbf{e}_p^T (A_p^T P_p + P_p A_p)\mathbf{e}_p. \tag{71}$$

Substituting the Lyapunov equations yields

$$\dot{V}(\mathbf{e}) = -\mathbf{e}_e^T \mathbf{e}_e - \mathbf{e}_p^T \mathbf{e}_p. \tag{72}$$

Thus,

$$\dot{V}(\mathbf{e}) = -\|\mathbf{e}\|^2 < 0, \quad \forall \mathbf{e} \neq \mathbf{0}. \tag{73}$$

Since $V(\mathbf{e})$ is positive definite, radially unbounded, and $\dot{V}(\mathbf{e})$ is strictly negative definite, according to Theorem 1 (Lyapunov's Direct Method [24]), the tracking error equilibrium point $\mathbf{e} = \mathbf{0}$ is globally asymptotically stable.

### 5.2. Elevation

In this section, a control law for trajectory tracking of the elevation subsystem of the tandem helicopter is proposed. Equation (74) shows the structure of the linear error model employed, where both the desired trajectories and the actual subsystem trajectories are incorporated.

$$\begin{bmatrix} \dot{\zeta}_d - \dot{\zeta} \\ \dot{\theta}_{ed} - \dot{\theta}_e \\ \ddot{\theta}_{ed} - \ddot{\theta}_e \end{bmatrix} = \begin{bmatrix} 0 & 1 & 0 \\ 0 & 0 & 1 \\ 0 & 0 & 0 \end{bmatrix} \begin{bmatrix} \zeta_d - \zeta \\ \theta_{ed} - \theta_e \\ \dot{\theta}_{ed} - \dot{\theta}_e \end{bmatrix} + \begin{bmatrix} 0 \\ 0 \\ 1 \end{bmatrix} [\varphi_e - v_b] \tag{74}$$

where $\zeta_d$ and $\theta_{ed}$ correspond to the desired reference trajectories, and $\varphi_e = \ddot{\theta}_{ed}$ represents the feedforward reference acceleration. The previous expression can be rewritten in compact state-space form as shown in Equation (75), demonstrating that the system dynamics remain linear in the error space:

$$\dot{e}_e = A_e e_e + B_e v_e \tag{75}$$

where $e_e = [\zeta_d - \zeta, \theta_{ed} - \theta_e, \dot{\theta}_{ed} - \dot{\theta}_e]^T$ is the error state vector, and $v_e$ represents the auxiliary control input.

The auxiliary control input $v_e$ is defined as $v_e = \varphi_e - v_b$, where $v_b$ is the feedback control law that stabilizes the error dynamics and drives the system toward the desired trajectory. Equation (76) presents the closed-loop feedback structure for $v_b$:

$$v_b = K_e e_e \tag{76}$$

where $K_e$ corresponds to the LQR feedback gain matrix obtained in Equation (40). Consequently, the complete auxiliary control input is expressed as $v_e = \varphi_e - K_e e_e$.

$$u_b = \frac{J_e}{l_a k} \left( \frac{l_w f_g}{J_e} \cos\theta_e + \varphi_e - K_e e_e \right) \tag{77}$$

The reference $\theta_{ed}$ used for trajectory tracking in the elevation subsystem corresponds to a periodic trapezoidal signal characterized by an upper position of 18 [deg] and a lower position of 2 [deg], with rise and fall times of 3 s and a dwell time of 16 s at each reference level.

This type of signal is proposed to emulate elevation or descent maneuvers in the presence of obstacles during a potential aerial mission, thereby allowing evaluation of the trajectory tracking capability and response time of the subsystem under abrupt changes in elevation position.

In Figure 9, the comparison between the desired trajectory (red dashed line) and the helicopter response in the elevation variable (blue solid line) is presented. The results show that the proposed control strategy effectively guides the aerial vehicle along the desired path, exhibiting maximum overshoots of 1.9979 [deg] at the upper and lower direction change points. Despite these minor transient peaks, the entire response remains strictly within the physical operating limits of the elevation axis, demonstrating high tracking efficiency and smooth closed-loop behavior.

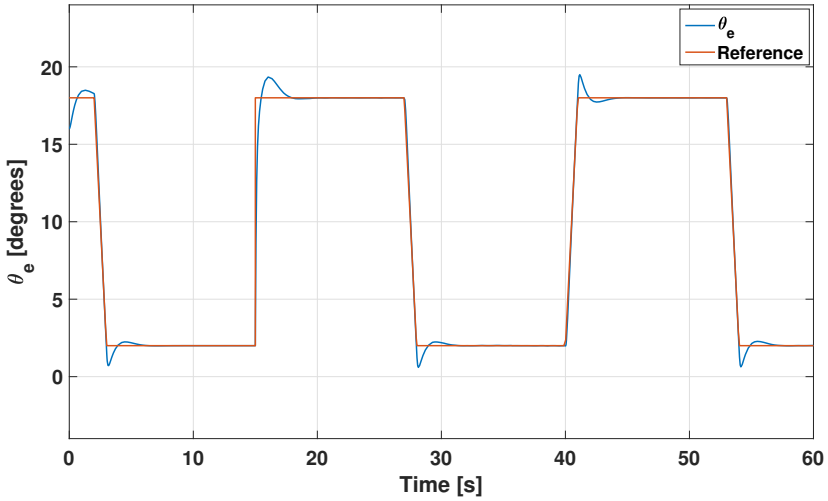
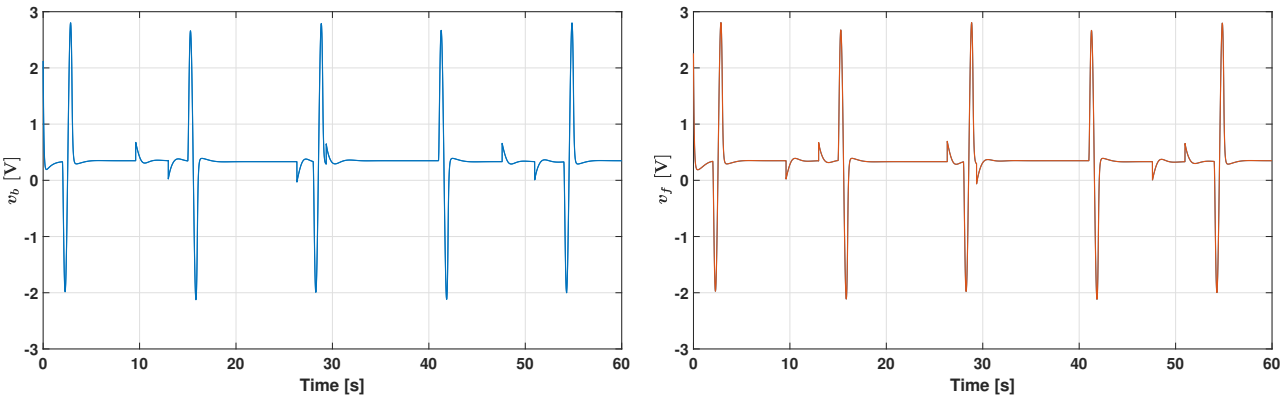



**Figure 9.** Trajectory tracking for the elevation state of the 3-DOF helicopter with initial conditions $\theta_e(0) = 16$ [deg], $\theta_p(0) = 0$ [deg], $\theta_t(0) = 0$ [deg], $\dot{\theta}_e(0) = 0$ [deg/s], $\dot{\theta}_p(0) = 0$ [deg/s], and $\dot{\theta}_t(0) = 0$ [deg/s], assuming constant system parameters.

Figure 10 shows the time evolution of the control voltages $v_b(t)$ and $v_f(t)$ throughout the 60 s simulation. The response demonstrates a coordinated periodic behavior between the actuators, characterized by sharp transient peaks reaching maximums of $+2.8$ V and minimums of $-2.1$ V during abrupt trajectory transitions. Minor impulses ($\approx \pm 0.6$ V) associated with secondary corrections can also be observed. In the intervals between reference changes, both control signals swiftly return to a stable steady-state level of $+0.34$ V. Notably, the peak values remain well below the maximum operating voltage of 5 V specified in Table 1, demonstrating the controller's ability to handle repetitive maneuvers without saturating the power stages or exhibiting drift.




(**a**) (**b**)

**Figure 10.** Motor voltage response during elevation trajectory tracking for the 3-DOF tandem helicopter: (**a**) Rear motor voltage. (**b**) Front motor voltage.

### *5.3. Pitch*

For the trajectory tracking design of the pitch motion, the transformed linear system presented in Equation (36) is employed. The desired reference vector in the transformed state space $z_d = [z_{1d}, z_{2d}, z_{3d}, z_{4d}]^T$ is obtained directly by mapping the desired physical

trajectories through the linearizing diffeomorphic transformation. Equation (78) details the proposed canonical error model structure:

$$\begin{bmatrix} \dot{z}_{1d} - \dot{z}_1 \\ \dot{z}_{2d} - \dot{z}_2 \\ \dot{z}_{3d} - \dot{z}_3 \\ \dot{z}_{4d} - \dot{z}_4 \end{bmatrix} = \begin{bmatrix} 0 & 1 & 0 & 0 \\ 0 & 0 & 1 & 0 \\ 0 & 0 & 0 & 1 \\ 0 & 0 & 0 & 0 \end{bmatrix} \begin{bmatrix} z_{1d} - z_1 \\ z_{2d} - z_2 \\ z_{3d} - z_3 \\ z_{4d} - z_4 \end{bmatrix} + \begin{bmatrix} 0 \\ 0 \\ 0 \\ 1 \end{bmatrix} \begin{bmatrix} \varphi_p - v \end{bmatrix} \tag{78}$$

where $v$ represents the auxiliary control input and $\varphi_p = z_{1d}^{(4)}$ represents the fourth derivative of the desired trajectory in the transformed domain. The previous system can be rewritten in compact state-space form as

$$\dot{e}_p = A_p e_p + B_p v_p \tag{79}$$

where $e_p = z_d - z$ corresponds to the tracking error vector in the transformed space. The auxiliary control input $v_p$ is designed incorporating both the feedforward acceleration term and the LQR state feedback law:

$$v_p = \varphi_p - v \tag{80}$$

and

$$v_p = -K_t e_p \tag{81}$$

where $K_t = [k_{t0}, k_{t1}, k_{t2}, k_{t3}]$ is the LQR feedback gain vector. Finally, by substituting $v_p$ into the fourth component of the transformed canonical model and solving for the physical input $u_f$, the explicit control law applied to the actuators is obtained:

$$u_f = \frac{(\varphi_p - K_t e_p) - \frac{l_a k_p}{J_t} x_4^2 \sin x_3}{\frac{l_a k_p}{J_t} \frac{l_h k}{J_p} \cos x_3} \tag{82}$$

Once again, a periodic trapezoidal reference signal is proposed $\theta_{pd}$, characterized by an upper position of 30 [deg] and a lower position of $-30$ [deg], with rise and fall times of 3 s. The dwell time at the lower extreme of the signal is 13 s, while at the upper position it is 17 s.

Figure 11 illustrates the response of the nonlinear subsystem under the designed trajectory tracking control law. In this simulation, a non-zero initial condition is considered ($\theta_p(0) = 28.75$ [deg]), requiring the controller to drive the helicopter toward the reference signal and subsequently maintain it along the desired path. It can also be observed that the maximum overshoot during direction changes, in both upper and lower directions, is 2.2059 [deg]. This highlights the excellent performance of the proposed control law, as the output signal remains well within the operational physical bounds of $\pm 32$ [deg], even though the desired trajectory operates in close proximity to this physical boundary.

As depicted in Figure 12, the control effort required during pitch trajectory tracking displays a significantly smaller magnitude compared to the elevation degree of freedom. While the motor voltages for elevation vary between $-2.1$ V and $+2.8$ V, the pitch commands demand much lower actuation effort, remaining well within $[0\text{ V}, 0.75\text{ V}]$ with transients between 0.05 V and 0.75 V. This highlights that pitch attitude adjustments require substantially less control energy, while both degrees of freedom operate comfortably within the physical actuator bounds ($\pm 5$ V).

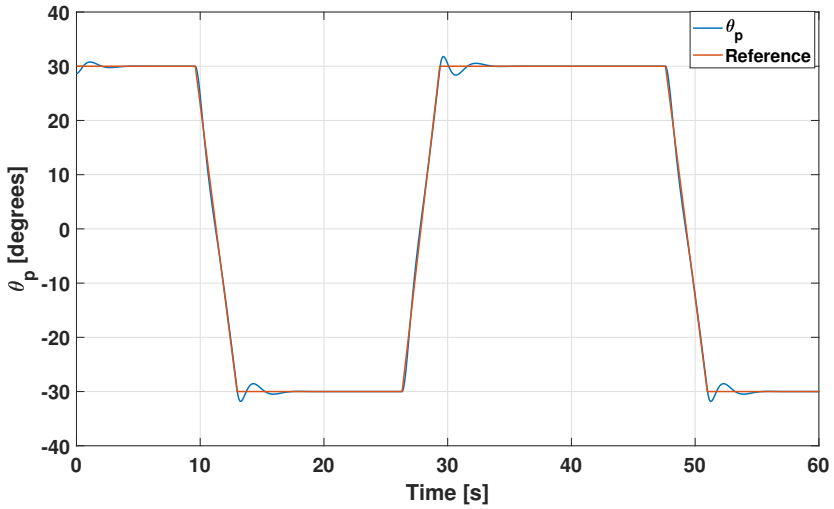
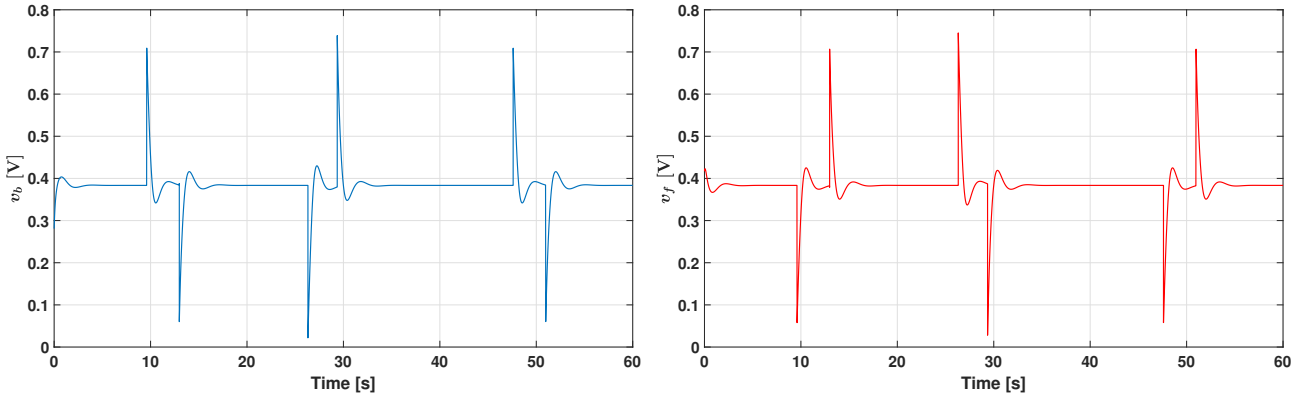



**Figure 11.** Trajectory tracking for the pitch state of the 3-DOF helicopter with initial conditions $\theta_e(0) = 0$ [deg], $\theta_p(0) = 28.75$ [deg], $\theta_t(0) = 0$ [deg], $\dot{\theta}_e(0) = 0$ [deg/s], $\dot{\theta}_p(0) = 0$ [deg/s], and $\dot{\theta}_t(0) = 0$ [deg/s], assuming constant system parameters.




(**a**) (**b**)

**Figure 12.** Motor voltage response during pitch trajectory tracking for the 3-DOF tandem helicopter: (**a**) Rear motor voltage. (**b**) Front motor voltage.

### *5.4. Travel*

Finally, the trajectory tracking control law for the travel degree of freedom is presented. Although the pitch and travel axes are physically coupled in the original nonlinear model, the diffeomorphic transformation completely decouples their dynamics. Consequently, the linear canonical system structure introduced in Equation (36) is employed, where the transformed reference vector $z_d = [z_{1d}, z_{2d}, z_{3d}, z_{4d}]^T$ is mapped from the desired travel trajectory.

Equation (83) details the decoupled canonical error model structure for the travel subsystem:

$$\begin{bmatrix} \dot{z}_{1d} - \dot{z}_1 \\ \dot{z}_{2d} - \dot{z}_2 \\ \dot{z}_{3d} - \dot{z}_3 \\ \dot{z}_{4d} - \dot{z}_4 \end{bmatrix} = \begin{bmatrix} 0 & 1 & 0 & 0 \\ 0 & 0 & 1 & 0 \\ 0 & 0 & 0 & 1 \\ 0 & 0 & 0 & 0 \end{bmatrix} \begin{bmatrix} z_{1d} - z_1 \\ z_{2d} - z_2 \\ z_{3d} - z_3 \\ z_{4d} - z_4 \end{bmatrix} + \begin{bmatrix} 0 \\ 0 \\ 0 \\ 1 \end{bmatrix} [\varphi_t - v] \tag{83}$$

where $v$ represents the auxiliary control input and $\varphi_t = z_{1d}^{(4)}$ denotes the fourth-order feedforward reference acceleration.

The travel tracking error dynamics can be expressed in compact state-space form as

$$\dot{e}_t = A_p e_t + B v_t \tag{84}$$

where $e_t = z_d - z$ is the travel error vector, $A_p$ corresponds to the 4th-order canonical matrix defined in Equation (79), and $B = [0, 0, 0, 1]^T$.

The auxiliary control input $v_t$ is constructed by combining the feedforward term with the LQR state feedback law:

$$v_t = \varphi_t - v \tag{85}$$

and

$$v_t = -K_t e_t \tag{86}$$

where $K_t = [k_{t0}, k_{t1}, k_{t2}, k_{t3}]$ is the LQR feedback gain vector synthesized specifically for the travel subsystem parameters. Finally, input $u_f$ the explicit control function applied to the actuators is obtained:

$$u_f = \frac{(\varphi_t - K_t e_t) - \frac{l_a k_p}{J_t} x_4^2 \sin x_3}{\frac{l_a k_p}{J_t} \frac{l_h k}{J_p} \cos x_3} \tag{87}$$

For the reference trajectory $\theta_{td}$, a periodic trapezoidal signal is proposed, characterized by an upper position of 30 [deg] and a lower position of $-30$ [deg], with rise and fall times of 3 s. The dwell time at the lower extreme of the signal is 13 s, while at the upper position it is 17 s.

Figure 13 presents a comparison between the reference signal (red dashed line) and the trajectory followed by the helicopter (blue solid line). It can be observed that the proposed control law effectively tracks the desired path, displaying moderate overshoots resulting from the abrupt positive and negative step changes in the reference signal. Furthermore, the controller rapidly drives the trajectory of the 3-DOF system toward the steady state, where it remains stable. It is worth emphasizing that for the travel state, the physical operational capability is an unconstrained 360 [deg] range; within this regime, the controller operates properly, exhibiting maximum overshoots and undershoots of up to 10.0518 [deg] during sharp reference transitions.

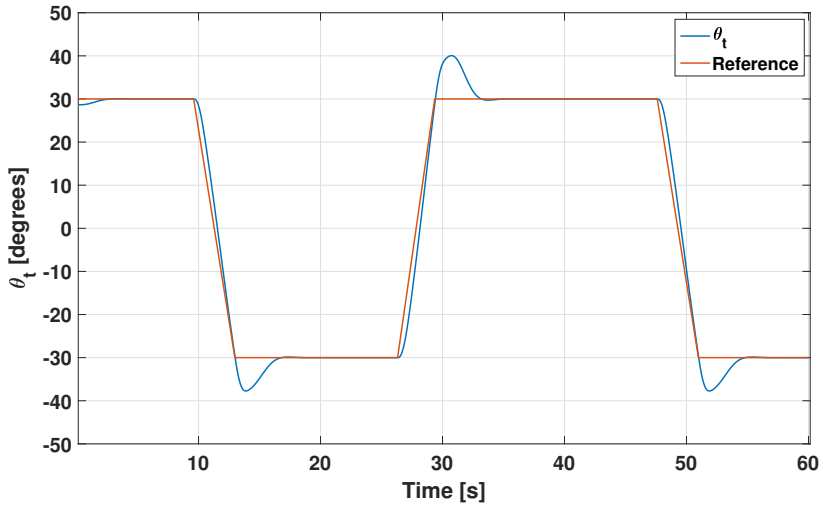
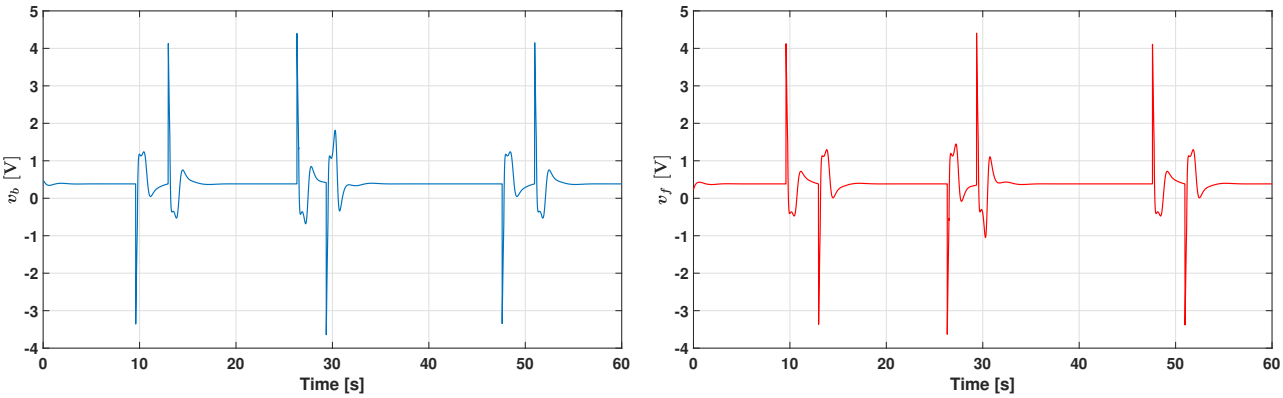



**Figure 13.** Trajectory tracking for the travel state of the 3-DOF helicopter with initial conditions $\theta_e(0) = 0$ [deg], $\theta_p(0) = 0$ [deg], $\theta_t(0) = 28.65$ [deg], $\dot{\theta}_e(0) = 0$ [deg/s], $\dot{\theta}_p(0) = 0$ [deg/s] and $\dot{\theta}_t(0) = 0$ [deg/s], assuming constant system parameters.

The dynamic response of the required control signal for the proposed exact feedback linearization and tracking scheme is shown in Figure 14. Figures 14a and 14b show the time responses of the back motor voltage ($v_b$) and front motor voltage ($v_f$), respectively. The fast voltage spikes observed at reference transitions are inherently driven by the feedforward acceleration terms required for aggressive trajectory tracking, reaching bounded extrema between $-3.6$ V and 4.4 V. These values remain well within the operational limit of $\pm 5$ V, ensuring that no actuator saturation occurs. Once the system settles, the control inputs quickly stabilize to baseline operating levels, demonstrating the practical feasibility and smooth performance of the control law under steady-state conditions.




(**a**) (**b**)

**Figure 14.** Motor voltage response during travel trajectory tracking for the 3-DOF tandem helicopter: (**a**) Rear motor voltage. (**b**) Front motor voltage.

To provide a quantitative assessment of the trajectory-tracking performance, the dynamic responses presented in Figures 9, 11 and 13 were evaluated using the root-mean-square error (RMSE), maximum absolute tracking error, settling time, and steady-state error. The resulting quantitative tracking performance metrics for each degree of freedom are summarized in Table 3.

**Table 3.** Quantitative trajectory tracking performance of the 3-DOF tandem helicopter.

| Figure | Variable | RMSE | Maximum Error | Settling Time | Steady-State Error |
|---|---|---|---|---|---|
| Figure 9 | Elevation (deg) | 0.6699 | 1.9979 | 0.4067 | 0.5515 |
| Figure 11 | Pitch (deg) | 0.5796 | 2.2059 | 1.9410 | 0.0590 |
| Figure 13 | Travel (deg) | 3.2168 | 10.0518 | 3.5020 | 0.0901 |

The reported metrics were calculated directly from the simulation data corresponding to each figure.

The quantitative metrics in Table 3 confirm the tracking capability and effective axis decoupling achieved by the proposed controller. While elevation and pitch exhibit rapid transient convergence, the travel axis experiences a larger transient excursion due to physical coupling and inertial forces, which are effectively dampened by the feedback control law to maintain steady-state tracking errors below 0.6 [deg] across all states.

In Figure 9, the elevation response ($\theta_e$) achieves rapid convergence under step transitions with a settling time of 0.4067 s and a maximum tracking error of 1.9979 [deg], yielding an overall RMSE of 0.6699 [deg] and a steady-state error of 0.5515 [deg]. For the pitch angle ($\theta_p$) in Figure 11, the state closely follows the trapezoidal reference with minimal corner oscillations (maximum error of 2.2059 [deg], settling time of 1.9410 s), resulting in a low RMSE of 0.5796 [deg] and a negligible steady-state error of 0.0590 [deg]. Finally, the travel state ($\theta_t$) in Figure 13 exhibits an inertial overshoot during ramp transitions (maximum

error of 10.0518 [deg], RMSE of 3.2168 [deg]), but stabilizes within 3.5020 s to reach a low steady-state error of 0.0901 [deg], confirming long-term positioning robustness.

## 6. Conclusions

In this work, a control strategy based on exact feedback linearization was presented for a Quanser 3-DOF tandem helicopter. Starting from the nonlinear dynamic model of the system, a symmetric transformation was employed to decouple the dynamics, and the resulting subsystems were analyzed independently.

The relative degree analysis and Lie distribution calculations verified that the subsystem containing the pitch and travel dynamics is involutive and can be exactly linearized, yielding a transformation that represents the system as a pure chain of integrators. By canceling the nonlinearities and designing appropriate control gains, the system was stabilized and the internal dynamics were guaranteed to remain stable. Additionally, the proposed strategy enabled trajectory tracking for obstacle avoidance in the elevation, pitch, and travel motions.

The results obtained demonstrate that exact feedback linearization is an effective tool for controlling nonlinear aerial systems with coupled dynamics. Furthermore, although the control law derived for the pitch and travel dynamics exhibits a singularity at $\theta_p = \pm\pi/2$, the mechanical constraints of the platform strictly prevent the controller from reaching these critical values. Finally, future work envisions extending the proposed approach to account for model uncertainties, external disturbances, and physical hardware experimentation. Additionally, future research will focus on analyzing key motor metrics to evaluate overall system efficiency and performance.

**Author Contributions:** Conceptualization, J.G.A.-A., S.A.R.-P., J.M.-M., B.B.S.-Q. and J.M.G.-V.; methodology, J.G.A.-A., S.A.R.-P., J.M.-M., B.B.S.-Q. and J.M.G.-V.; software, J.G.A.-A., S.A.R.-P., J.M.-M. and J.M.G.-V.; validation, J.G.A.-A., S.A.R.-P. and J.M.-M.; formal analysis, J.G.A.-A., S.A.R.-P. and J.M.-M.; investigation, J.G.A.-A., S.A.R.-P., J.M.-M., B.B.S.-Q. and J.M.G.-V.; resources, J.G.A.-A., S.A.R.-P., J.M.-M., B.B.S.-Q. and J.M.G.-V.; data curation, S.A.R.-P. and J.M.-M.; writing—original draft preparation, J.G.A.-A. and S.A.R.-P.; writing—review and editing, J.G.A.-A., S.A.R.-P., J.M.-M. and J.M.G.-V.; visualization, J.G.A.-A., S.A.R.-P. and J.M.-M.; supervision, J.G.A.-A. and S.A.R.-P.; project administration, S.A.R.-P.; funding acquisition, S.A.R.-P. All authors have read and agreed to the published version of the manuscript.

**Funding:** This research was supported by the Secretariat of Science, Humanities, Technology and Innovation (SECIHTI) of Mexico through the postgraduate scholarship awarded to Jorge Guillermo Alonso Alfaro (Grant No. 394339).

**Data Availability Statement:** This article includes all original contributions of the study. For any further information, inquiries should be directed to the corresponding author.

**Acknowledgments:** The authors acknowledge the National Polytechnic Institute (IPN) and SECIHTI for the support provided in carrying out this research work.

**Conflicts of Interest:** The authors declare no conflicts of interest.

## References

1. Agencia Federal de Aviación Civil. Norma Oficial Mexicana NOM-107-SCT3-2019. In *Diario Oficial de la Federación*; Agencia Federal de Aviación Civil: Ciudad de México, Mexico, 2019.
2. Singh, C.; Gatti, R.R. *Drone Applications for Industry 5.0*; IGI Global: Hershey, PA, USA, 2024.
3. Tarr, A.A.; Tarr, J.A.; Thompson, M.; Ellis, J. *Drone Law and Policy*; Taylor & Francis: Abingdon, UK, 2021.
4. Virués-Ortega, D.; García-Cabañas-Bueno, J.A.; Vergara-Merino, R.; Bernardo-Sanz, S.; Hernández-Correas, A.; Ramos-Campo, D. *Piloto de Dron (RPAS)*; Ediciones Paraninfo: Madrid, Spain, 2016.

5. García-Carrillo, L.R.; Dzul-López, A.E.; Lozano, R.; Pégard, C. *Quad Rotorcraft Control: Vision-Based Hovering and Navigation*; Springer: London, UK, 2013.
6. García-Cabañas-Bueno, J.A.; Hernández-Correas, A.; Ramos-Campo, D. *Curso Modular de Piloto de Dron (UAS)*; Ediciones Paraninfo: Madrid, Spain, 2022.
7. Aladro-Marín, J.D. Estrategia de Control Multimodo Para Convertiplano con Propulsión Basculante. Ph.D. Thesis, Universidad Autónoma de Nuevo León, Monterrey, Mexico, 2021.
8. Fernández, J.; Vilas, A.A.; Bustingorry, D.; Heidenreich, E. El Método de los Elementos Finitos Aplicado a UAV. *Ingenium* **2017**, *4*, 6–11.
9. Pajares, G.; Ruz, J.J.; Lanillos, P.; Guijarro, M.; de la Cruz, J.M. Generación de trayectorias y toma de decisiones para UAVs. *Rev. Iberoam. Automática Informática Ind.* **2008**, *5*, 83–92. [CrossRef]
10. Sisk, S.; Du, X. Surrogate-Based Multidisciplinary Optimization for Drone Takeoff. *Processes* **2024**, *12*, 1864. [CrossRef]
11. Wang, X.; Tan, G.Z.; Lu, F.L.; Zhao, J.; Dai, Y.S. Optimal Deployment Algorithm for UAV Swarms. *Processes* **2020**, *8*, 369. [CrossRef]
12. González-Morgado, A.; Álvarez Cía, C.; Heredia, G.; Ollero, A. UAV Fully-Actuated: Modelo, Control y Comparación. *Rev. Iberoam. Automática Informática Ind.* **2023**, *20*, 401–411. [CrossRef]
13. Quanser Inc. *User Manual: 3DOF Helicopter Experiment*; Quanser Inc.: Markham, ON, Canada, 2012.
14. Boukhnifer, M.; Chaibet, A.; Larouci, C. H-Infinity Robust Control of 3-DOF Helicopter. In Proceedings of the International Multi-Conference on Systems, Signals and Devices, Chemnitz, Germany, 20–23 March 2012.
15. Peng, C.; Zhu, B.; Yin, L.; Yang, B.; Wang, C. Attitude Synchronization of Multiple 3-DOF Helicopters. In Proceedings of the Chinese Control Conference, Hangzhou, China, 28–30 July 2015; pp. 7196–7201. [CrossRef]
16. Zhu, B.; Liu, H.H.T.; Li, Z. Robust Distributed Attitude Synchronization. *Control Eng. Pract.* **2015**, *36*, 87–99. [CrossRef]
17. Capello, E.; Punta, E.; Fridman, L.M. Sliding Mode Control for a 3-DOF Helicopter. In Proceedings of the IEEE Conference on Decision and Control, Las Vegas, NV, USA, 12–14 December 2016; pp. 6464–6469. [CrossRef]
18. Assunção, E.; Teixeira, M.C.M.; Buzachero, L.F.S.; da Silva, E.R.P. Switched Optimal Robust Control of a 3-DOF Helicopter. In Proceedings of the IEEE International Conference on Industry Applications (INDUSCON), Curitiba, PR, Brazil, 20–23 November 2016. [CrossRef]
19. Castañeda, H.; Plestan, F.; Chriette, A.; de Leon-Morales, J. Continuous Differentiator Based on Adaptive Second-Order Sliding-Mode Control for a 3-DOF Helicopter. *IEEE Trans. Ind. Electron.* **2016**, *63*, 5786–5793. [CrossRef]
20. Isidori, A. *Nonlinear Control Systems*; Springer: Berlin/Heidelberg, Germany, 1995. [CrossRef]
21. Sira-Ramírez, H. *Control de Sistemas no Lineales*; Pearson Education: London, UK, 2005.
22. Rodríguez-Paredes, S.A. Análisis Estructural de un Modelo de Helicóptero. Master's Thesis, Centro de Investigación y Estudios Avanzados del IPN, Ciudad de México, Mexico, 1999.
23. Rodríguez-Paredes, S.A.; Mondié, S.; Martínez-García, J.C. A Structure-Based Methodology for Block Decoupling: A Case Study. In Proceedings of the Proceedings of the American Control Conference, Chicago, IL, USA, 28–30 June 2000; pp. 394–398.
24. Khalil, H.K. *Nonlinear Systems*, 3rd ed.; Prentice Hall: Upper Saddle River, NJ, USA, 2002.


**Disclaimer/Publisher's Note:** The statements, opinions and data contained in all publications are solely those of the individual author(s) and contributor(s) and not of MDPI and/or the editor(s). MDPI and/or the editor(s) disclaim responsibility for any injury to people or property resulting from any ideas, methods, instructions or products referred to in the content.